Slow oscillations of dispersion-managed solitons

H. Hartwig, M. Böhm, A. Hause, and F. Mitschke*
Universität Rostock, Institut für Physik, D-18051 Rostock, Germany†
(Received 23 October 2009; published 8 March 2010)

In dispersion-managed fibers, soliton-like solutions with periodically recurring shapes exist. These so called dispersion-managed solitons are relevant for fiber-optic telecommunication. In this article we address their behavior when there is deviation from the stationary solution, which is accompanied by the excitation of a long-lived periodic oscillation. We give a possible interpretation by applying soliton radiation beat analysis, a method capable of analyzing the soliton content.

DOI: 10.1103/PhysRevA.81.033810 PACS number(s): 42.81.Dp, 42.65.Tg

I. INTRODUCTION

The concept of solitons in optical fibers was originally demonstrated in 1980 by Mollenauer *et al.* [1]. For several years now the soliton concept has found its way into optical fiber telecommunication. In recent schemes, however, fibers of periodically alternating dispersion are employed; this has benefits like suppression of nonlinear mixing effects (four-wave mixing) and Gordon-Haus timing jitter. When viewed stroboscopically with the dispersion map period [2], pulses maintain their shape. Note that just as in constant-dispersion fibers, in these dispersion-managed fibers a balance of nonlinearity and dispersive effects stabilizes the pulse shapes over the long haul. Therefore these pulses are called dispersion-managed (DM) solitons.

It is well-known that for alternating dispersion the fundamental soliton no longer has a hyperbolic secant shape. Instead, it may more closely resemble a Gaussian shape [3,4] at least near its center, while characteristic dips may appear in the pulse slopes. Within each dispersion map period, the pulse width breathes due to the local variations of dispersion. At the end of each dispersion map period, the pulse reaches its initial amplitude and phase profile (apart from a constant phase offset) The amount of breathing is related to the so-called map strength S which depends on the amount of dispersion variation and the pulse bandwidth. Among the several slightly different definitions in use we adhere to the one given in [5].

Although there is no known closed analytic expression for the stationary pulse in general, a numerical representation can be obtained by iterative procedures (see, e.g., [6–9]). Moreover, Lushnikov [10–12] derived an asymptotic expression, and Hundertmark and Lee [13] found analytic constraints on the pulse shape.

Of course, pulses in real world systems never precisely match the pulse shape of (stroboscopically) stationary DM solitons. Therefore, the impact of deviations from the stationary case is of practical interest. It has been observed in numerical simulations and variational models that upon perturbation there is no exact recurrence of the pulse shape after a full dispersion map period: instead, undulations of the pulse shape over many dispersion map periods have been noticed (which we refer to as slow oscillations).

This subject has been studied by several authors with various methods. Kivshar *et al.* [14] and Pelinovsky *et al.* [15] treat the slow oscillations in the context of internal modes of solitons in nonintegrable systems. Kutz *et al.* [16] observed a slow oscillation based on a variational approach and in numerical simulations. Using the same variational model, Turitsyn *et al.* [17] determined optimized pulse parameters and the slow oscillation amplitude. Lakoba and Pelinovsky [18] apply the concept of internal modes to describe slow oscillations in dispersion-managed fibers and point out that there are odd and even internal modes. Tonello [19] developed the solution of the nonlinear Schrödinger equation in terms of Hermite-Gauss modes, which also yielded slow oscillations. Capobianco *et al.* [20] and Tonello *et al.* [21] characterized the dynamics of DM solitons using a linear stability analysis. In a different approach, a phase plane representation for the nonstationary return-to-zero pulse propagation was given by Mookherjea [22].

The use of a variational ansatz, perturbation theory, etc., requires a careful check of its limits of applicability. Assumptions are being made (e.g., about the period of the slow oscillation being much longer than the dispersion map period). Here we adopt a quite different approach and present a systematic, assumption-free numerical analysis of the slow oscillations.

This article is organized as follows: We begin with a parameter set at which slow oscillations are readily observed. We proceed by analyzing this oscillation in terms of its spatial frequency spectrum. By an analogy to the well-known case of the $N = 2$ soliton of the nonlinear Schrödinger equation, the result suggests an interpretation in terms of internal constituent solitons. We expand the analysis by considering other parameter ranges and different perturbations. Finally we discuss the relation of this interpretation to that in the literature in terms of internal modes. Our procedure exactly reproduces all frequencies obtained from internal modes, but goes beyond.

II. PHYSICAL MODEL

In this article, the governing equation is the nonlinear Schrödinger equation (NLSE) with alternating dispersion,

$$\frac{\partial}{\partial z}A = -\frac{i}{2}\beta_2(z)\frac{\partial^2}{\partial T^2}A + i\gamma|A|^2 A, \qquad (1)$$

*fedor.mitschke@uni-rostock.de
†URL: www.physik.uni-rostock.de/optik

where $A = A(T, z)$ denotes the complex-valued envelope of the light field as a function of propagation distance z and time T in a co-moving frame of reference. γ is the Kerr nonlinearity parameter, and $\beta_2(z)$ is the piecewise constant group velocity dispersion parameter. For the sake of clarity of the basic concept we restrict ourselves to this simplest case. Higher-order dispersion, Raman effect, polarization effects, loss or gain, etc., are neglected but may be included if of interest from a practical point of view.

Numerical simulation of Eq. (1) is carried out using the symmetrized split-step Fourier transform method. The parameters are chosen to be similar to those in the experimental setup in [5]. The nonlinear coefficient is $\gamma = 2.3\,\mathrm{W}^{-1}\,\mathrm{km}^{-1}$ throughout. The lengths of both fibers involved are $L^+ = L^- = 10$ m such that the dispersion map period is $L = 20$ m. The normal dispersion fiber has a dispersion of $\beta_2^+ = 49\ \mathrm{ps}^2/\mathrm{km}$, and the anomalous dispersion fiber has a dispersion of $\beta_2^- = -51\ \mathrm{ps}^2/\mathrm{km}$. This yields a path-average dispersion of

$$\bar{\beta}_2 = \frac{L^+\beta_2^+ + L^-\beta_2^-}{L} = -1.0\ \mathrm{ps}^2/\mathrm{km}. \qquad (2)$$

We let the fiber line begin and end with a half segment of anomalous dispersion fiber. This way, the chirp-free point should always occur at segment midpoints [17].

III. NUMERICAL ANALYSIS OF SLOW OSCILLATIONS

In order to analyze the slow oscillations, we start with the set of parameters given previously and leave the pulse energy as a scan parameter. For each energy, we generate an initial pulse shape for a single-humped solution by using the iterative procedure given in [7]. This provides, as best as possible, the precise (unperturbed) stationary pulse shape of the DM soliton. This initial pulse shape is launched at the midpoint of the anomalous dispersion fiber, and its propagation is computed by solving Eq. (1) numerically. We start with the case of a pulse energy of 10 pJ (for other values, see Sec. VII).

Propagation reveals breathing of the pulse shape in the dispersion map period as expected. Figure 1(a) shows a Fourier transform of the evolution of spectral power density $\tilde{P}(z) = |\tilde{A}(\omega_0, z)|^2$ at the center optical frequency, evaluated for a fiber length of 6000 dispersion map periods L, at 32 equidistant points per period. Center optical frequency is $\omega_0 = 2\pi c/\lambda$ with c being the speed of light and $\lambda = 1.56\ \mu$m.

Figure 1(b) shows an enlarged portion near the first harmonic. In the upper part the case of the unperturbed initial pulse shape as just discussed is shown. For the lower part we perturbed the pulse shape by scaling the initial field amplitude $A(T, z = 0)$ of the stationary solution by a constant factor $1 + \epsilon$ with $\epsilon \ll 1$. Note that by this procedure only a symmetric perturbation is generated; for antisymmetric perturbations see Sec. VIII. As comparison of Fig. 1(b), panels (i) and (ii) reveals, the perturbation away from the precise stationary pulse shape generates several fairly strong sidebands. It stands to reason that for a perfectly stationary solution (if it exists) even the remnant sidebands in panel (i) would disappear.

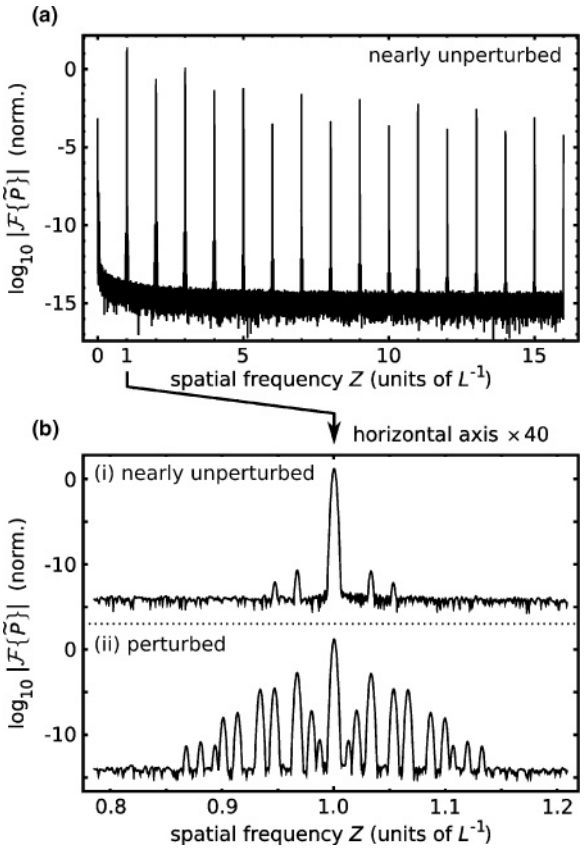

FIG. 1. (a) Spectrum of spatial frequencies of full propagation data of (nearly) unperturbed DM soliton solution. The period of the dispersion map and its integer multiples occur. (b) Enlarged section for the propagation of (nearly) unperturbed and perturbed DM soliton solutions.

IV. ANALYSIS OF STROBOSCOPICALLY SAMPLED DATA

For a first reduction of complexity without loss of relevant information we take samples only at intervals equal to the dispersion map period. This is known as the stroboscopic representation; it is equivalent to a Poincaré section [23]. As the representative position we take the midpoint in the anomalous dispersion fiber segment. We convinced ourselves that taking samples at other positions does not alter the obtained information. Figure 2 shows the evolution of the spectral power density $\tilde{P}$ at center optical frequency ω_0 over 1000 dispersion map periods for a pulse perturbed slightly away from the stationary case. The slow oscillation here has a period of ≈30 dispersion map periods. It is hard to judge by inspection, though, whether the oscillation has a sinusoidal shape. Therefore we analyze the data of Fig. 2 by Fourier transform. The result is displayed in Fig. 3, where the dominant slow oscillation appears at $Z = 1/(30\,L) \approx 0.033\,L^{-1}$. As expected, the data in Fig. 3 give the same information as the data in Fig. 1(b), panel (ii), with the advantage of reduced complexity in data aquisition.

For further analysis it will be helpful to analyze not only data taken at the center optical frequency but also data taken off center. This requires a different format of graphical representation introduced in Fig. 4. The horizontal axis represents optical frequency referred to as center frequency

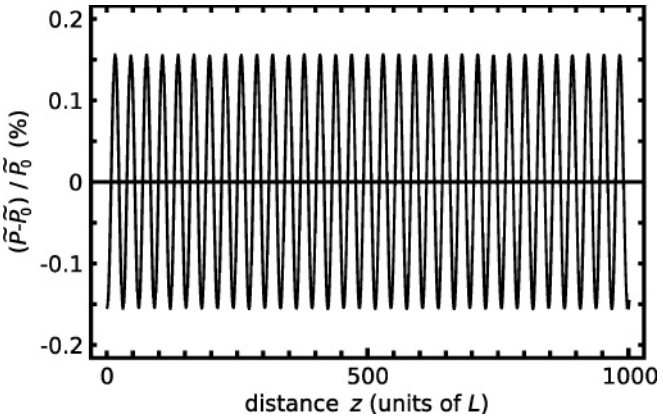

FIG. 2. Evolution of the central spectral power density $\tilde{P}$. Shown is the deviation from the stationary solution. Data are sampled stroboscopically at the midpoint of the anomalous dispersion fiber segment.

(here, all optical frequencies are given as angular frequencies). The vertical axis repeats the horizontal (spatial frequency) axis of Fig. 2; in fact, the data from that figure can be found along the center vertical. The Fourier transform of the spectral power density yields the spatial frequency spectrum; its absolute value is indicated by gray scale. Note that some of the lines are interrupted at locations located symmetrically around the center optical frequency. At these locations, the amplitude of the slow oscillations goes through zero, and the phase of the slow oscillation reverses its sign.

An interpretation of this fairly complex picture is considerably simplified if one first considers the equivalent representation of a well-known case. By way of comparison, an explanation of the various spectral features is given. We therefore first turn to a discussion of the second-order soliton of the ordinary (constant dispersion) NLSE.

V. A WELL-KNOWN CASE

The $N = 2$ soliton of the NLSE is well understood to consist of two fundamental solitons coexisting at the same temporal position and with the same center frequency, with energies at a ratio of 3:1. This has been shown by inverse

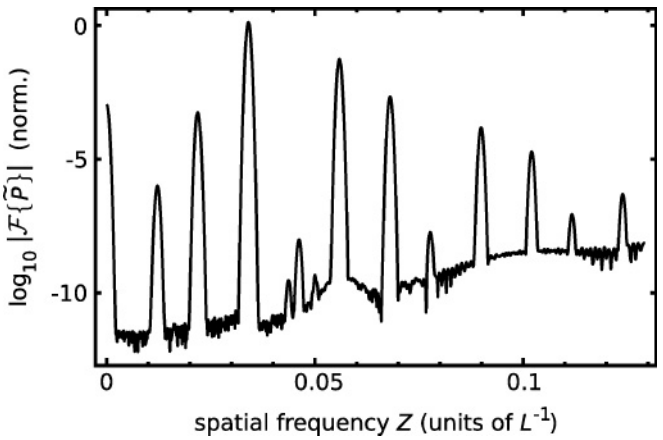

FIG. 3. Fourier transform of the slow oscillation in Fig. 2. Several spatial frequency components can be discerned.

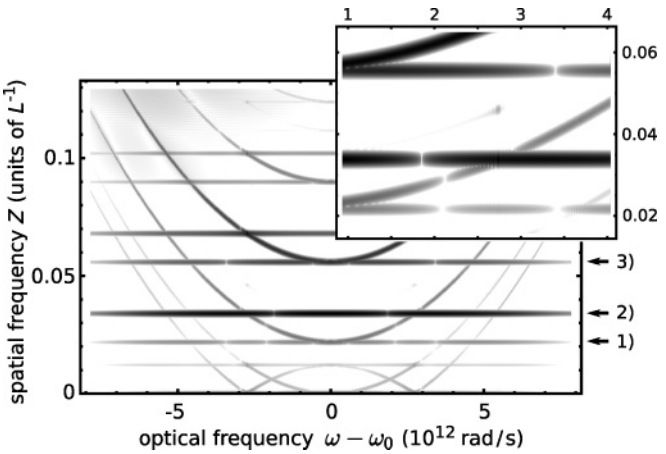

FIG. 4. Fourier transform of spectral power density as a function of optical frequency. Grey scale corresponds to log of Fourier signal. Labels are explained in the text.

scattering theory in [24,25]. Since the phase rotation rate of a soliton depends on its energy, these rates are given by

$$\frac{\partial\phi_1^{\mathrm{sol}}}{\partial z} = 9\frac{\beta_2}{2\,T_0^2}, \tag{3}$$

$$\frac{\partial\phi_2^{\mathrm{sol}}}{\partial z} = \frac{\beta_2}{2\,T_0^2}, \tag{4}$$

for the higher and lower energy soliton, respectively (compare [26]). These rates are independent of optical frequency.

Now we use spatial frequencies which are given in terms of the phase rotation rate by

$$Z = \frac{1}{2\pi}\frac{\partial\phi}{\partial z}. \tag{5}$$

One finds that the phase in Eq. (4) rotates an entire 2π after a distance of $4\pi T_0^2/\beta_2 = 8z_0$, where z_0 is usually called the soliton period because the power profile actually recurs already every z_0 [27]. This becomes clear by considering the difference of phase between Eqs. (3) and (4) which rotates 8 times more rapidly.

When the launch condition does not correspond to an exact $N = 2$ soliton, in addition to the solitons, a dispersive background is generated which is commonly referred to as radiation. Its phase will evolve according to

$$\frac{\partial\phi^{\mathrm{disp}}}{\partial z} = \frac{1}{2}\beta_2\,(\omega-\omega_0)^2\,, \tag{6}$$

with ω being the optical frequency and ω_0 the center value.

Recently a procedure called soliton radiation beat analysis (SRBA) was introduced which systematically evaluates such beat notes to obtain information about the soliton content of solitary waves [26]. The method allows one to disentangle beat notes, both between several solitons and between solitons and radiation. Specifically, SRBA uses some representative variable of the pulse evolution as input; the spectral power density at center, sampled along the propagation, is a good choice. (In the temporal domain radiation disperses away, and beat contrast degrades. In the spectral domain, contrast

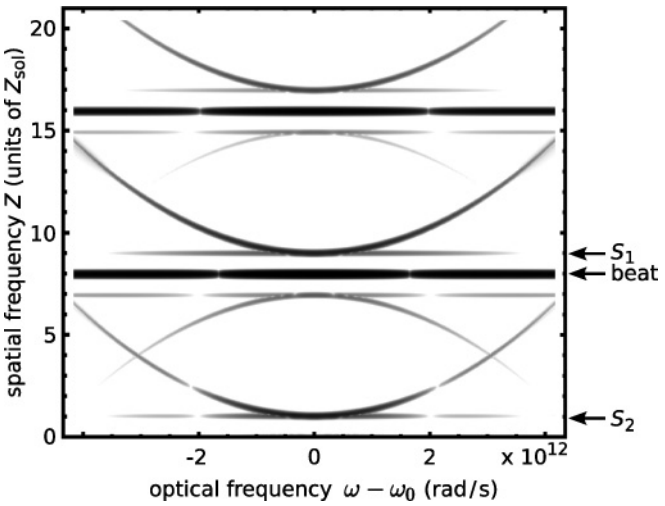

FIG. 5. Beat frequencies for the case that a second-order soliton co-propagates with a dispersive wave. Gray scale corresponds to log of Fourier transform of spectral power density. Spatial frequency unit is $Z_{sol} = 1/(8z_0)$. Arrows labeled S_1 and S_2 mark the value of phase evolution for the first and second soliton; their beat note is labeled "beat."

is maintained.) If, in analogy to the above, other optical frequencies are also included, a representation as shown in Fig. 5 is obtained. Here, the launch condition corresponded to $N = 2.01$; that is, the exact $N = 2$ soliton was scaled by an amplitude factor of 1.005.

In Fig. 5, spatial frequencies are given in units of $Z_{sol} = 1/(8z_0)$. The lower-energy fundamental soliton has spatial frequency $Z = 1\,Z_{sol}$. (This would be exact for the exact $N = 2$ launching condition; however, the difference is minimal and irrelevant for our argument.) Spatial frequency scales as the square of the energy; that of the higher-energy fundamental soliton is therefore found at $Z = 9\,Z_{sol}$. Both positions are highlighted in Fig. 5. A beat note between these two at $Z = 8\,Z_{sol} = 1/z_0$ reproduces the soliton period z_0.

More horizontal lines in Fig. 5 are explained as harmonics and mixing frequencies of the above. The radiation background, by virtue of the quadratic dependence in Eq. (6), yields parabolic curves; mixing products with the soliton signals give rise to the parabolas visible in Fig. 5. They are tangent to the soliton signals at center optical frequency. There is a certain ambiguity about which horizontal lines correspond to solitons, which are beat notes between them and which are overtones and combination tones. However, all lines related to solitons touch a parabola at center frequency (from the apex of the parabolas, the color of the respective soliton can be read). The line at $Z = 8\,Z_{sol}$ stands out by not doing that; this must be a beat between solitons, and the line at $Z = 16\,Z_{sol}$ is its overtone. The picture therefore allows the conclusion that there are two solitons of the same frequency ("color"), with energy 1 and 3 units, plus radiation. This is exactly what is known.

VI. INTERPRETATION

We now compare Fig. 5 for the ordinary $N = 2$ soliton with the corresponding Fig. 4 in the DM case. The phase evolution of the dispersive wave Eq. (6) also holds for the case of dispersion management when β_2 is replaced by the path average value $\bar{\beta}_2$. It is therefore not surprising that the parabolas look much the same. A straightforward interpretation would then be that two constituent solitons of the same center frequency (color) appear at $Z = 0.022\ L^{-1}$ and $Z = 0.055\ L^{-1}$. They form a beat at $Z = 0.033\ L^{-1}$, which manifests itself as the observed slow oscillation. DM solitons thus show features like those found in multisoliton states. As a consequence, the DM soliton studied here at 10 pJ could be viewed as a second-order DM soliton; it's existence has already been demonstrated in [26] using a different ansatz. We comment later in this article on the relation of this interpretation with that in terms of internal modes. However, in order to be able to discuss the relation fully we first need to consider the situation at various energies (solitons appear at thresholds!) and for different kinds of perturbations.

VII. ENERGY DEPENDENCE, SYMMETRIC PERTURBATION

The previous analysis was carried out for an energy of $E = 10$ pJ. We now extend our analysis to the range of $1.0 \leqslant E \leqslant 20.5$ pJ. As long as symmetric perturbations are considered, it suffices to evaluate the evolution of spectral amplitude at center optical frequency. We increment the energy in steps of 0.5 pJ and find the pulse shape for the stationary solution at each step. We then vary the pulse shape around this solution by an amplitude scale factor so that the energy is varied by ± 0.25 pJ in steps of 0.05 pJ; this way the intervals have one point of overlap, providing a convenient sanity check. Note that this procedure creates a perturbation that is symmetric.

Figure 6 shows the result. The Fourier transforms of spectral power densities are displayed on a logarithmic gray scale. At each incremental step there is a vertical gap (apparent white line). This was expected because the stationary pulse shape should not produce beats. For energies off the stationary cases numerous oscillation frequencies appear which, in their entirety, reveal distinct branches: frequencies which continuously vary with energy.

For the sake of clarity, we redraw the figure with continuous branches in Fig. 7; the gray scale is standardized to a discrete set of line styles. For each energy value shown, all frequencies can be described as mutual combination frequencies (overtones, sum and difference frequencies). For example, below 3 pJ, there is one frequency (line labeled S_1) plus its first and second overtone. Then, in the range between 3 and 11 pJ, a new branch (labeled S_2) emerges from zero, while at the same point S_1 splits into three branches, etc. In this range, there is no obvious *a priori* criterion for which of the branches may be fundamental and which secondary (combination tone). At 11 pJ, a similar situation occurs with the advent of S_3.

Adopting the interpretation above, three solitons appear near 0 pJ, at 3 pJ, and at 11 pJ, respectively. Combination frequencies Z_j of these solitons, given by

$$Z_j = \left| \sum_i c_i S_i \right|, \quad \text{with } c_i = 0, \pm 1, \pm 2, \ldots, \tag{7}$$

fully explain all branches of Figs. 6 and 7 without any further assumptions.

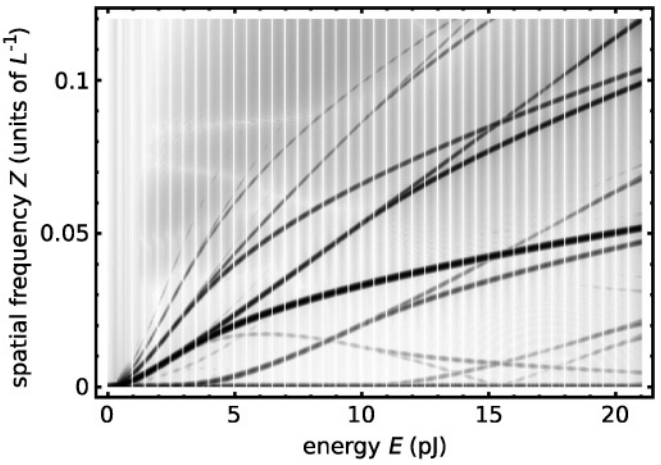

FIG. 6. Density plot of amplitudes of spatial frequency components as a function of pulse energy. Spatial frequencies are given in units of inverse dispersion map periods, L^{-1}. At increments of 0.5 pJ stationary DM soliton solutions were used; hence the gaps. At neighboring points spatial frequency components are revealed.

There are independent checks of whether the line labeled S_1 stands for the first soliton. If one launches a single stationary soliton in a numerical simulation and follows its phase evolution, one directly obtains the S_1 curve. Moreover, we also indicated the curve for the fundamental soliton in a homogenous fiber of the same path-average dispersion (labeled "sol"). In the limit of low energy the map strength goes to zero, and both curves must coincide—which they obviously do.

We repeat that by construction we introduced only symmetric perturbations of the pulses; therefore we now turn to the case of asymmetric perturbations.

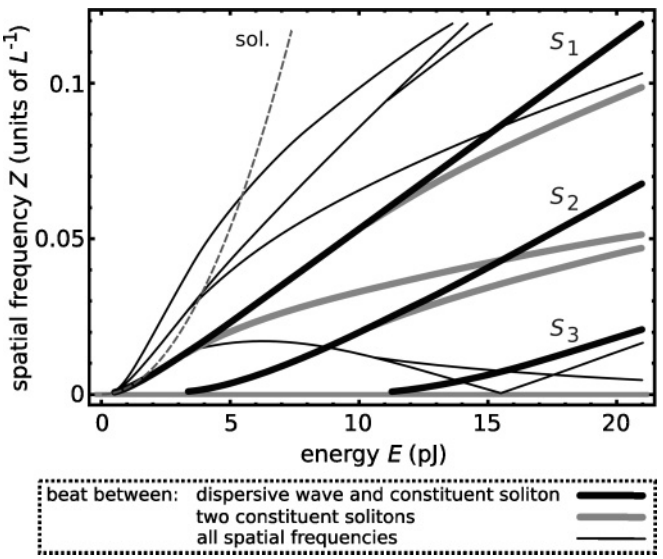

FIG. 7. Redrawn version of Fig. 6 to aid the interpretation. If one interprets lines labeled $S_{1...3}$ as three constituent solitons, all other frequencies are explained as combination frequencies or overtones thereof. The dashed curve labeled "sol" gives the phase evolution of a fundamental soliton in a homogeneous fiber.

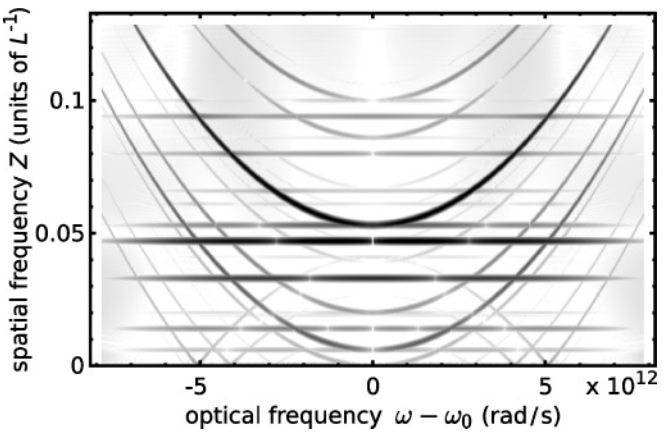

FIG. 8. Fourier transform of spectral power density as a function of optical frequency for the case of asymmetric perturbation. Gray scale corresponds to log of Fourier signal.

VIII. ENERGY DEPENDENCE, ASYMMETRIC PERTURBATIONS

In this section we use the same incremental steps of energies as before, but introduce the perturbation in a different way: To generate a pulse asymmetry without affecting the far wings we use the derivative of a Gaussian of the same width as the pulse itself and add it to the pulse with 0.01 amplitude weight. We convinced ourselves that this particular choice of shape and amplitude coefficient is uncritical. Instead, noise can be added to yield the same information. This procedure reveals all possible slow oscillations.

In this asymmetric case the number of frequencies is increased over the symmetric case. We therefore need to go back to the format used in Fig. 4, now shown in Fig. 8.

Note that again, as in the case of symmetric perturbation, the amplitudes can have zeros. However, such zeros may now also occur at zero detuning. At each of the zeros, the phase of slow oscillation changes by π. Here, because of these zeros, data extraction can no longer be limited to center optical frequency. Instead, we need to carry the whole picture.

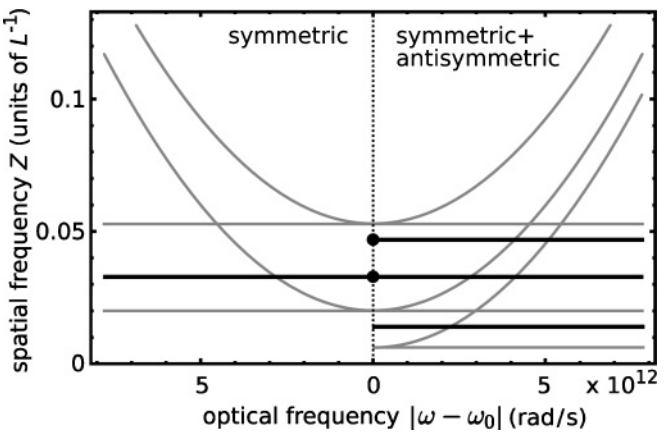

FIG. 9. Comparison of DM soliton at 10 pJ with initial perturbations of different symmetry. The two spatial frequencies marked with the dots can also be calculated using the method in [21]. The full information about the spatial frequencies, as shown here, is obtained by means of Fourier transform.

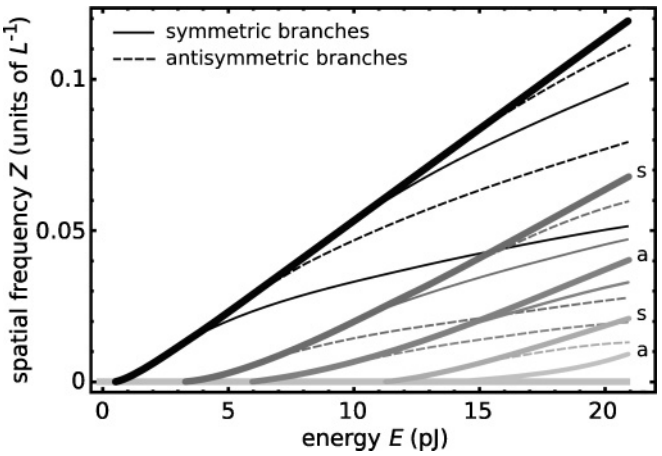

FIG. 10. Spatial frequency components visible upon symmetric perturbation (s) and antisymmetric perturbation (a).

For better clarity, we juxtapose the essence of Figs. 4 and 8 in Fig. 9. Obviously, with the asymmetric perturbation all branches from the symmetric case are still there, but additional lines appear. It seems fair to attribute these to antisymmetric perturbation. This is consistent with the observation that these are precisely the lines with a zero amplitude at center optical frequency.

After all symmetric and antisymmetric branches are identified, we can compose them in a format like that in Fig. 7; this is shown in Fig. 10. In the interest of clarity, higher harmonics were omitted. Comparison reveals that in addition to the branches $S_{1\ldots3}$ beginning near 0 pJ, at 3 pJ, and at 11 pJ there are now additional branches emerging at 6 and 14 pJ, respectively. The former are labeled "s" (symmetric); the latter are labeled "a" (antisymmetric). Note that they appear alternatingly when energy is increased.

IX. CONCLUSIONS

As stated previously, slow oscillations of DM solitons have been analyzed by other authors with various methods [14–22]. To date, only one method—linear stability analysis—has been applied to analyze the DM soliton oscillation frequencies as a function of energy [20,21]. As a result, the occurrence of branches of even or odd symmetry emerging from the boundary toward a continuous spectrum of slow oscillations was reported. In contrast to analytical approaches the method presented here carries the whole information about the system, even for strong perturbations. For the time being, our focus is on frequency information; amplitude information might provide further insights.

Our analysis reveals that there are further slow oscillation frequencies that were not seen in [20,21] (compare Fig. 9). We want to emphasize that these additional frequencies are inherent to the system and are not an artifact of the method. Thus one can say that the Fourier-transform-based SRBA method provides a more complete picture of the slow oscillations of the DM soliton.

When the influence of local dispersion variation is small (this is the case for pulses with low energy), both linear stability analysis and SRBA show that the slow oscillations of DM solitons resemble the case of solitons in homogeneous fibers: in either case there is just a single phase evolution plus overtones, visible when beating with radiation. Once the local dispersion modulation significantly influences the pulse dynamics (which is the case for more elevated energies), the stationary DM solitons inherently have a set of oscillation frequencies, in contrast to ordinary (fundamental) solitons.

We showed that a straightforward interpretation is to attribute these slow oscillations to a beat between phase evolutions of constituent solitons. In this sense the description of the DM soliton as a composite object goes beyond a description in terms of internal modes. It should be clear that the composite character does not imply a linear superposition because the system is inherently nonlinear. Above we have used an analogy with the $N = 2$ soliton of the NLSE; in that case the constituent solitons can be separated under certain conditions [28]. Whether a similar separation can also be performed here must at present remain unresolved.

[1] L. F. Mollenauer, R. H. Stolen, and J. P. Gordon, Phys. Rev. Lett. **45**, 1095 (1980).
[2] N. J. Smith, F. M. Knox, N. J. Doran, K. J. Blow, and I. Bennion, Electron. Lett. **32**, 54 (1996).
[3] I. Gabitov, E. G. Shapiro, and S. K. Turitsyn, Phys. Rev. E **55**, 3624 (1997).
[4] N. J. Smith, N. J. Doran, W. Forysiak, and F. M. Knox, J. Lightwave Technol. **15**, 1808 (1997).
[5] M. Stratmann, T. Pagel, and F. Mitschke, Phys. Rev. Lett. **95**, 143902 (2005).
[6] M. J. Ablowitz and G. Biondini, Opt. Lett. **23**, 1668 (1998).
[7] J. H. B. Nijhof, W. Forysiak, and N. J. Doran, IEEE J. Sel. Top. Quantum Electron. **6**, 330 (2000).
[8] R. K. Jackson, C. K. R. T. Jones, and V. Zharnitsky, Physica D **190**, 63 (2004).
[9] P. Y. P. Chen, P. L. Chu, and B. A. Malomed, Opt. Commun. **245**, 425 (2005).
[10] P. M. Lushnikov, Opt. Lett. **25**, 1144 (2000).
[11] P. M. Lushnikov, Opt. Lett. **26**, 1535 (2001).
[12] P. M. Lushnikov, J. Opt. Soc. Am. **21**, 1913 (2004).
[13] D. Hundertmark and Y.-R. Lee, Commun. Math. Phys. **286**, 851 (2009).
[14] Y. S. Kivshar, D. E. Pelinovsky, T. Cretegny, and M. Peyrard, Phys. Rev. Lett. **80**, 5032 (1998).
[15] D. E. Pelinovsky, Y. S. Kivshar, and V. V. Afanasjev, Physica D **116**, 121 (1998).
[16] J. N. Kutz, P. Holmes, S. G. Evangelides, and J. P. Gordon, J. Opt. Soc. Am. B **15**, 87 (1998).
[17] S. K. Turitsyn, J. H. B. Nijhof, V. K. Mezentsev, and N. J. Doran, Opt. Lett. **24**, 1871 (1999).
[18] T. I. Lakoba and D. E. Pelinovsky, Chaos **10**, 539 (2000).

[19] A. Tonello, J. Opt. A: Pure Appl. Opt. **2**, 338 (2000).
[20] A.-D. Capobianco, G. Nalesso, A. Tonello, F. Consolandi, C. D. Angelis, and F. Gringoli, Opt. Lett. **28**, 1754 (2003).
[21] A. Tonello, A.-D. Capobianco, G. Nalesso, F. Gringoli, and C. D. Angelis, Opt. Commun. **246**, 393 (2005).
[22] S. Mookherjea, IEEE J. Sel. Top. Quantum Electron. **12**, 497 (2006).
[23] P. Bergé, Y. Pomeau, and C. Vidal, *Order within Chaos* (Wiley & Sons, New York, 1984).
[24] V. E. Zakharov and A. B. Shabat, Sov. Phys. JETP **34**, 62 (1972).
[25] J. Satsuma and N. Yajima, Suppl. Prog. Theor. Phys. **55**, 284 (1974).
[26] M. Böhm and F. Mitschke, Phys. Rev. E **73**, 066615 (2006).
[27] G. P. Agrawal, *Nonlinear Fiber Optics* (Elsevier, Amsterdam/New York, 2007), 4th ed.
[28] E. A. Golovchenko, E. M. Dianov, A. M. Prokhorov, and V. N. Serkin, JETP Lett. **42**, 87 (1985).